

VIII- II -1. Project Research

Project 1

PR1 Irradiation Effects on Microstructural Evolution in Materials Irradiated by Particles with High Energy

Q. Xu

Research Reactor Institute, Kyoto University

OBJECTIVES: Neutron irradiations in KUR have been used to not only estimate degradation mechanical properties of materials but also develop new materials, such as material for optoelectronic and high-power devices. In addition, other irradiation facilities, such as ions, electrons and γ rays, have also been used in the present project research to clarify the damage structural development.

RESULTS: The allotted research subject (ARS) and the name of co-researches in each ARS are listed below. Ferritic steels containing Cr are expected to be used for the first-wall component in fusion reactors. Neutron irradiation induced phase separation in Fe-30Cr binary alloy. Transmutation of ^{14}C , which related luminescence and net carrier concentration, in GaN by a (n, p) reaction of ^{14}N was reported. Others results are presented in detail in this progress reports.

ARS-1

Neutron-transmuted Carbon-14 in neutron-irradiated GaN compensation of DX-like center

(K. Kuriyama, T. Ida, K. Kamioka, K. Kushida, and Q. Xu)

ARS-2

Neutron irradiation effects of superconducting magnet materials at low temperature

(T. Nakamoto, M. Yoshida, T. Ogitsu, Y. Makida, K. Yoshimura, S. Mihara, K. Sasaki, M. Sugano, H. Nishiguchi, M. Iio, Y. Kuno, M. Aoki, A. Sato, T. Itahashi, Q. Xu, K. Sato, Y. Kuriyama, Y. Mori and T. Yoshiie)

ARS-3

Study on formation and recovery processes of radiation damage in crystalline materials

(A. Kinomura, K. Sato, Q. Xu and T. Yoshiie)

ARS-4

Blue emission of natural calcite by gamma rays

(T. Awata, Y. Bando and Q. Xu)

ARS-5

Annealing behavior of thermal diffusivity in ceramics irradiated by 30 MeV electron and neutron

(M. Akiyoshi, I. Takagi, T. Yoshiie, Q. Xu, K. Sato)

ARS-6

Annealing behavior of vacancy-type defects in Mg-Zn-Y alloy with LPSO structure introduced by electron-irradiation at liquid nitrogen temperature

(Y. Nagai, K. Inoue, T. Toyama, Y. Matsukawa, Y. Shimizu, A. Kuramoto, H. Takamizawa, Y. Kakubo, T. Yoshiie, Q. Xu and K. Sato)

ARS-7

Radiation damage in bulk amorphous alloys by electron irradiation

(F.Hori, N. Onodera, A.Ishii, S.Mineno, A.Iwase, Y. Yokoyama, Q.Xu, K.Sato and T.Yoshiie)

ARS-8

Development of replica extraction method for vanadium alloys and its application for neutron-irradiated ones

(K. Fukumoto and Q. Xu)

ARS-9

Damage evolution in neutron-irradiated metals during neutron irradiation at elevated temperatures

(I.Mukouda, K. Yamakawa, T. Yoshiie, Q. Xu)

ARS-10

Positron annihilation behavior of Fe-Cr alloys after neutron irradiation in KUR

(R. Kasada, K. Sato, Q. Xu, T. Yoshiie)

ARS-11

Similarity of radiation resistance of nanocrystalline Ni by ion and neutron irradiation

(H. Tsuchida, A. Itoh, K. Sato, T. Yoshiie, Q. Xu)

ARS-12

Interaction between deuterium and defects in tungsten (2)

(K. Sato, R. Tamiya, Q. Xu and T. Yoshiie)

ARS-13

Irradiation effects on stress loading property of refractory metal at high temperature

(K. Tokunaga, K. Araki, T. Ukita, Q. Xu, T. Yoshiie)

ARS-14

Effect of substrate temperature in nanocell fabrication of GaSb

(N. Nitta, K. Yokoyama and M. Taniwaki)

ARS-15

Deuterium retention in electron-irradiated VPS-W

Y. Hatano, J. Shi, T. Nozaki, K. Masude, T. Tokunaga, H. Watanabe, N. Yoshida, K. Sato and Q. Xu

K. Kuriyama, T. Ida, K. Kamioka, K. Kushida¹ and Q. Xu²

College of Engineering and Research Center of Ion Beam Technology, Hosei University

¹Osaka Kyoiku University

²Research Reactor Institute, Kyoto University

INTRODUCTION: In our previous study [1], we reported that Ge atoms were transmuted into Ga in GaN by a (n, γ) reaction of ⁶⁹Ga and ⁷¹Ga, which acted as donors. ¹⁴C atoms would be also transmuted from ¹⁴N in GaN by a (n,p) reaction of ¹⁴N. In the present study, we report the transmutation of ¹⁴C in GaN by a (n,p) reaction of ¹⁴N. The transmuted ¹⁴C related luminescence and net carrier concentration are studied by combining photoluminescence, liquid scintillation, and Raman scattering.

EXPERIMENTS: GaN single crystal films grown by metalorganic-vapor-phase epitaxy were irradiated with fast and thermal neutrons at fluxes of $3.9 \times 10^{13} \text{ cm}^{-2} \text{ s}^{-1}$ and $8.15 \times 10^{13} \text{ cm}^{-2} \text{ s}^{-1}$, respectively. Irradiation time was 48 hours. The calculated ⁷²Ge and ¹⁴C concentrations were $1.24 \times 10^{18} \text{ cm}^{-3}$ and $1.13 \times 10^{18} \text{ cm}^{-3}$, respectively.

RESULTS: The transmuted ¹⁴C was studied by the liquid scintillation method to detect β -rays emitted in the process of ¹⁴C decays from ¹⁴N. Tritium (³H) is also emitted by a (n,t) reaction of ¹⁴N due to the neutron irradiation above 4.5 MeV. Figure 1 shows the liquid scintillation spectra of NTD-GaN. The transmuted ³H concentration is three orders of magnitude lower than that of ¹⁴C. However, the radiation dose of the emitted ³H is ten times higher than that of ¹⁴C. This attributes to the difference of the half-life, namely ¹⁴C has a half-life of 5730 years, but that of ³H is 12.33 years. The short half-life elements release more radiation.

As shown in figure 2, photoluminescence relating to carbon [2], DX-like center of Ge [1], and yellow luminescence band (YL) relating to the crystal defects by fast neutron was observed in 1000 °C annealed NTD-GaN.

Figure 3 shows a Raman spectrum. The peaks at 421 cm^{-1} and 756 cm^{-1} are related to the sapphire substrate. The spectra relating to the NTD-GaN are observed at 740 cm^{-1} and 575 cm^{-1} . The free electron concentration (N) estimated from $N = 1.1 \times 10^{17} (\nu_{\text{max}} - 736)^{0.764}$ [3], where ν_{max} is the LO mode frequency, is $3.17 \times 10^{17} \text{ cm}^{-3}$. This value is lower than that from the transmuted Ge concentration. Therefore, the DX-like center of Ge [1] would be

compensated by the transmuted ¹⁴C acceptor.

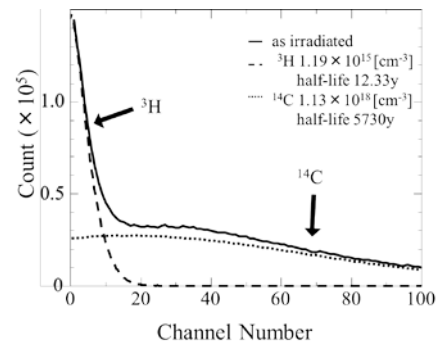


Fig 1. Liquid scintillation spectra of NTD-GaN.

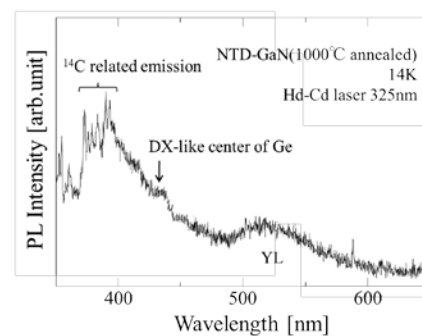


Fig 2. Photoluminescence spectra of 1000 °C annealed NTD-GaN.

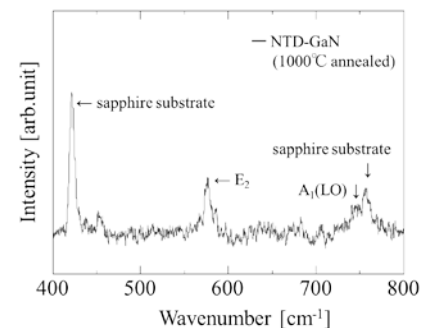


Fig 3. Raman spectra of 1000 °C annealed NTD-GaN.

REFERENCES:

- [1] K. Kuriyama, T. Tokumasu, J. Takahashi, H. Kondo, and M. Okada, Appl. Phys. Lett. **80**, (2002) 3328;
- [2] S. Fischer, C. Wetzel, and E. E. Haller, and B. K. Meyer, Appl. Phys. Lett. **67**, (1995) 1298.
- [3] C. Wetzel, W. Walukiewicz, E. E. Haller, J. Ager III, I. Grzegory, S. Porowski, and T. Suski, Phys. Rev. B **53**, (1996) 1322.

A part of this work was presented in 31th Int. Conf. Physics of Semiconductors in Zurich (2012, July. 30 ~ August. 2).

T. Nakamoto, M. Yoshida, T. Ogitsu, Y. Makida,
K. Yoshimura, S. Mihara, K. Sasaki, M. Sugano,
H. Nishiguchi, M. Iio, Y. Kuno¹, M. Aoki¹, A. Sato¹,
T. Itahashi¹, Q. Xu², K. Sato², Y. Kuriyama², Y. Mori²
and T. Yoshiie²

J-PARC Center, KEK

¹Department of Physics, Osaka University

²Research Reactor Institute, Kyoto University

INTRODUCTION: The superconducting magnets will be subjected to a high neutron fluence of 10^{21} n/m² or higher in the operation life time in the high energy particle physics experiments, such as a high luminosity upgrade of the LHC at CERN and the muon source for the COMET experiment at J-PARC. Since electrical resistivity of a stabilizer at low temperature, which is very sensitive to neutron irradiation, is one of the important parameters for the quench protection of the magnet system. A series of electrical resistivity measurement at neutron irradiation for the aluminum stabilizer with additives of yttrium taken from the prototype superconducting cable as well as copper stabilizer was started in 2011. In 2012, the second irradiation test with the same samples in 2011 was performed to observe the effect of the multiple irradiations and the thermal cycles to room temperature.

EXPERIMENTS: The irradiation tests have been carried out at a low temperature irradiation facility (LTL) at E-4 line of KUR. The aluminum stabilizer samples (RRR~350) with dimensions of 1 mm x 1 mm x 70 mm were cut from the superconducting cable manufactured by Hitachi Cable. The copper stabilizer sample (RRR~300) also has the same dimensions. The electric resistance was measured by a 4-wire method employing a Keithley 6221 current source and a Keithley 2182A voltmeter. The temperature was determined by using a thermocouple of Au(Fe) and Chromel, since the Cernox sensor (CX-1050-SD) showed a temperature drift during neutron exposure due to the irradiation damage. The thermocouple and the Cernox sensor and placed just behind the samples to measure the temperature of the helium gas coolant.

RESULTS: The second irradiation test for two aluminum samples (Al-Y1, Al-Y2) and one copper sample was carried out in Nov. 2012. The irradiation condition is basically same as the first irradiation in 2011. After cooling down to 13 K, the reactor was turned on to a power of 1 MW. The estimated fast neutron fluence in 52 hour operation is 2.6×10^{20} n/m². Resistance of the samples and temperature variations during the irradiation are shown in Fig. 1. The temperature jumped from 13 K to 15 K at the beginning due to radiation from the reactor

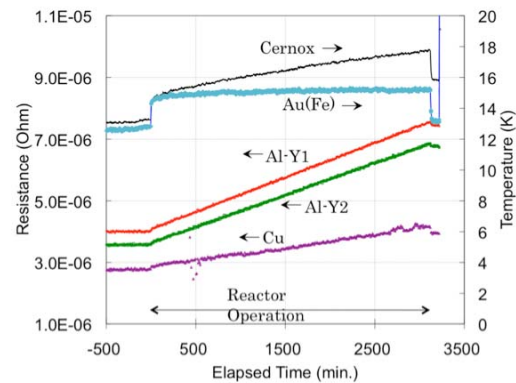


Fig.1. Electrical resistance of aluminum and copper stabilizer samples during the neutron irradiation in 2012.

core. During exposure the thermocouple indicates stable temperature while the Cernox sensor readout drifts up to 18 K due to irradiation damage. Behavior of the induced resistance by the neutron irradiation is very similar to the previous results in 2011: the resistance shows linear increase with respect to the neutron fluence during the exposure. Degradation rates of the electrical resistivity at the fluence of 10^{20} n/m² are 2.7×10^1 pΩm and 1.0×10^1 pΩm for the aluminum and the copper samples, respectively.

Anneal effects of the samples due to the thermal cycle to room temperature were observed. For the aluminum samples, the induced resistance was fully recovered to be the original resistance by the thermal cycles for the first and the second neutron irradiations. For the copper sample, however, the recovery of the resistance by the thermal cycle was imperfect. The recovery rates, defined as how much induced electrical resistivity due to the irradiation is recovered by the thermal cycle, were 84 % and 96 % for the first and the second irradiations, respectively. These results seem to be consistent with the previous works.

SUMMARY: A series of neutron irradiation tests have been pursued at KUR, with the aim of R&D for radiation hard superconducting magnets. The aluminum stabilizer with yttrium additive and the copper stabilizer from the superconducting cable were irradiated in 2011 and 2012 in order to investigate the multiple irradiation effects and the anneal effects by the thermal cycles on electrical resistivity. Each sample showed consistent resistivity increase in the first and the second irradiation runs. A full recovery of the resistivity was confirmed in the aluminum sample while the copper sample indicated the recovery rate of around 90 %.

A. Kinomura, K. Sato¹, Q. Xu¹ and T. Yoshiie¹

National Institute of Advanced Industrial Science and Technology (AIST)

¹ *Kyoto University Research Reactor Institute (KURRI)*

INTRODUCTION: Radiation effects of ion irradiation have been extensively studied for various materials. In general, radiation damage degrades crystallinity and gives harmful effects on material properties. However, under appropriate irradiation or annealing conditions, the radiation effects can induce interesting phenomena or useful structures in materials. A typical example of such effects is the ion beam annealing in Si, where implantation-induced damage layers are recrystallized by other ion irradiation. Thus, it is important to investigate the radiation effects of energetic particles (ions and neutrons) with materials.

EXPERIMENTS: Two types of experiments have been performed so far. As the first experiment, neutron enhanced annealing of ion-implantation induced damage in single-crystalline Si was studied. Si ion implantation to crystalline Si samples was performed at 200 keV to doses of $5 \times 10^{14} - 2 \times 10^{15} \text{ cm}^{-2}$ to induce radiation damage or amorphous phases. The damaged Si samples were neutron-irradiated in the KUR (Kyoto University Reactor) core or SSS irradiation facilities. The samples with and without neutron irradiation were characterized by Rutherford backscattering/channeling (RBS/C). As the second experiment, gettering of metal impurities to hydrogen-implanted multicrystalline Si was studied. The multicrystalline Si was implanted with 50 keV H^+ to a dose of $3 \times 10^{16} \text{ cm}^{-2}$ and annealed at 750 or 850 °C for 1h. The gettering effect of metal impurities was characterized by neutron activation analysis using the core or hydronuematic irradiation facilities of KUR.

RESULTS: In the neutron enhanced annealing experiments, annealing effects were negligible in the case of amorphized samples (with doses of 1 or $2 \times 10^{15} \text{ cm}^{-2}$). The heavily damaged samples (with a dose of $5 \times 10^{14} \text{ cm}^{-2}$) showed sufficient annealing effects for the core and SSS irradiations. The sample temperature of the SSS irradiation was accurately controlled at 400 °C. On the other hand, the sample temperature of the core irradiation cannot be measured during the neutron irradiation, although the water temperature in the KUR core can be measured. Thus it is important to estimate the sample

temperature of the irradiation capsule. We numerically solved one- or two-dimensional partial differential equation of heat flow for the Si sample in a KUR core irradiation capsule. The capsule consists of outer and inner sub-capsules made of Al. He gas was introduced in the capsule. The ambient temperature of the capsule was adjusted to the water temperature of the reactor core (49 °C in this calculation). Such information together with capsule and sample sizes was put in the calculation. Figure 1 shows the calculated temperature distributions (cross-sectional views) of the core irradiation capsule with Si samples. Fig. 1(a) and 1(b) assumed the circular and the rectangular sample shape with the same cross-sectional area. The maximum temperatures in the capsule were 85 and 81 °C for Fig. 1(a) and 1(b), respectively. From these calculations, the sample temperature during the neutron irradiation at the KUR core irradiation facility was estimated to be less than 90 °C. The RBS/C spectra of the control sample thermally annealed at 90 °C showed that the damage peak was bigger than that of the neutron irradiated sample. We confirmed that the neutron enhanced annealing occurred in the core irradiation as well as in the SSS irradiation at 400 °C. The specimen for cross-section TEM (transmission electron microscopy) for the gettering experiment was prepared by the FIB milling machine. The best milling condition was determined and the further sample preparation is in progress.

In summary, the sample temperature during neutron irradiation of the core irradiation facility was calculated. The FIB-milling condition for the multicrystalline Si sample for the gettering experiment was determined.

ACKNOWLEDGMENT: We would like to thank colleagues in AIST for their assistance on this study.

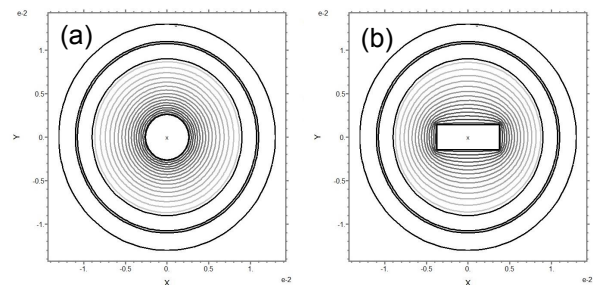


Fig. 1 Calculated temperature distributions (cross sectional views) inside the KUR core irradiation capsule with Si samples. The circular (a) and rectangular (b) shapes of the samples were assumed.

T. Awata, Y. Bando and Q. Xu¹

Department of Physics, Naruto University of Education
¹Research Reactor Institute, Kyoto University

INTRODUCTION: The calcite (CaCO_3) has been studied since 1940's because it has the possibility of radiation dosimeter [1]. In the past years, we reported thermoluminescence of natural calcite irradiated by gamma rays and it was shown that the spectra had only one orange emission peak at 620nm and that may be originated from impurity Mn^{2+} [2-3]. In this study, we have measured blue thermoluminescence emission of Mexico natural calcite and also have performed trace impurity elements analysis using NAA (Neutron Activation Analysis) and ICP-AES (Inductively Coupled Plasma Atomic Emission Spectroscopy) to clear the relationship with blue emission bands and impurities.

EXPERIMENTS: The sample is natural calcite at Mexico. It was irradiated ^{60}Co gamma rays for 1h (20kGy) at KUR and also irradiated neutron at Pn-3 of KUR for NAA. The gamma rays spectrum was taken by Ge detector at KUR after 1day for short-lifetime element and after two weeks for long-lifetime elements. ICP-AES (iCAP6300Duo, Thermo Fisher) was also performed to measure impurity elements concentration of Mexico calcite at KUR.

RESULTS and DISCUSSION: Figure 1 shows the thermoluminescence spectra of Mexico calcite irradiated gamma rays at 77K which are measured 93K to 413K

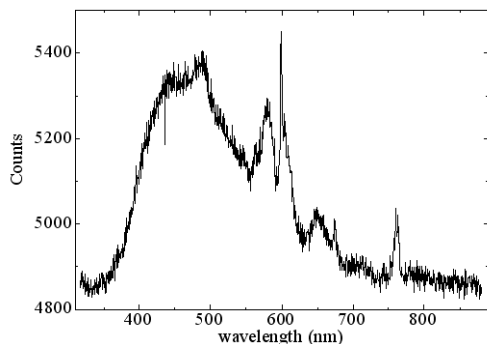


Fig. 1 Thermoluminescence spectrum of Mexico natural calcite irradiated by gamma rays.

with heating speed at 0.32K /sec. In this spectrum, there are seven peaks at 440nm, 487nm, 575nm, 600nm (line shape), 650nm, 675nm (line shape) and 760nm (doublet). Figure 2 and 3 show the gamma rays energy spectrum of Mexico natural calcite irradiated by neutron at Pn-3 for after 1 day and for after 14days, respectively. These figures showed that Fe, Mn, Na, La and Eu are detected in

the calcite. From ICP-AES results, impurities (ppm) of Fe(0.335), Mn(0.216), Na(1.31), Pb (0.0967), Pr(3.19) and Sm(0.0386) were contained in this calcite. A. Sidike et. al. [4] showed that photoluminescence peak of calcite at 487nm was related to impurity of Pb in calcite. Photoluminescence data reference [5] showed that emission peak at 575nm for impurity Eu and 610nm for Sm. From these results, peak at 487nm in figure 1 might be related to origin of Pb, 600nm peak to origin of Sm. Other peaks can not be assigned now.

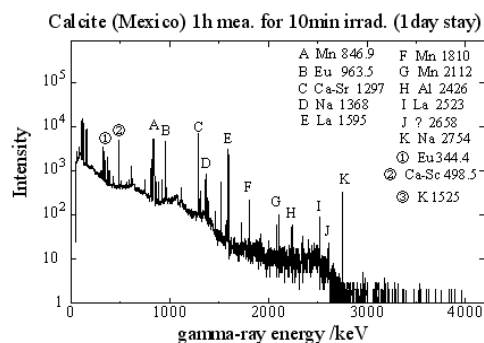


Fig. 2 Gamma-ray energy spectrum of Mexico natural calcite irradiated by neutron at Pn-3 for after 1 day.

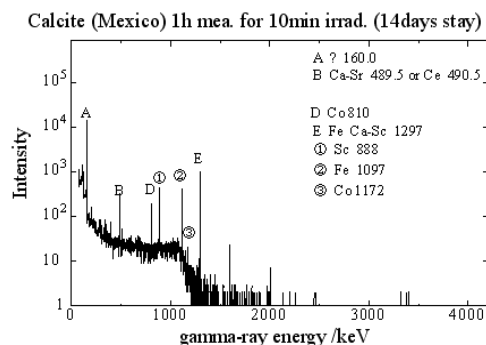


Fig.3 Gamma-ray energy spectrum of Mexico natural calcite irradiated by neutron at Pn-3 for after 14 days.

ACKNOWLEDGEMENT: We would like to thank Professor Dr. S. Fukutani (KURRI) for using ICP-AES on this study.

REFERENCES:

- [1] W. L. Medlin, *J. Opt. Soc. Am.* 53(1963) 1276-1285.
- [2] T. Awata and Q. Xu, KURRI Progress Report 2010 p.183.
- [3] T. Awata, T. Kishino, F. Maki and Q. Xu, KURRI Progress Report 2011 p.143.
- [4] A. Sidike, X. M. Wang, A. Sawuti, H. -J. Zhu, I. Kusachi and N. Yamashita, *Phys. Chem. Minerals*, **33** (2006) 559.
- [5] Colin M. MacRae and Nicholas C. Wilson, *Microsc. Microanal.* **14** (2008) 184.

M. Akiyoshi, I. Takagi, T. Yoshiie¹, Q. Xu¹ and K. Sato¹

Faculty of Engineering, Kyoto University

¹Research Reactor Institute, Kyoto University

INTRODUCTION:

It is well known that neutron-irradiated ceramics showed significant degradation in thermal diffusivity, while thermal diffusivity during the irradiation is still not estimated. A temperature of a specimen is calculated from the thermal conductivity easily, but at an irradiation condition, thermal conductivity of specimen decreased, and that rise the temperature of the specimen. The increased temperature anneals the irradiation induced defects, and that recover the thermal conductivity. To resolve this problem, kinetic analysis is required. In this analysis, most important information is the behavior of point defects.

EXPERIMENTS:

Accordingly, in this work, 30MeV electron accelerator KURRI-Linac is used to induce point-defects in bulk specimens of typical structural ceramics (AlN and β -SiC) to $1.5 \times 10^{24} \text{ e/m}^2$ which correspond to 0.01dpa. The irradiation was performed in the water-cooled specimen holder at around 80°C.

After the irradiation, isochronal annealing was conducted every 100°C up to 1100°C in vacuum using the SiC furnace of TC-7000H. Specimens were annealed for 1 h at an objective temperature. After the annealing, specimens were cooled in the furnace to the room temperature, and then thermal diffusivity was measured by the laser-flash method using a specially ordered measurement system (ULVAC Techno. TC-7000H/Special), and was analyzed with the $t_{1/2}$ method.

In addition, neutron-irradiations have been performed in the experimental fast reactor JOYO using CMIR-4 rig in previous works. The capsule T51 was irradiated to 28 dpa at 502°C and the capsule T57 was irradiated to 37 dpa at 738°C. These samples were also isochronal annealed up to 1500°C and measurements of thermal diffusivity were performed at room temperature.

RESULTS:

Figs. 1 and 2 show recovery behavior of the thermal diffusivity in the electron- and neutron-irradiated AlN and β -SiC ceramic specimens with isochronal annealing. The filled symbols in the figure represent the result from electron-irradiated specimen, and their thermal diffusivities were shown with left-side axis. The error bar shows standard deviation among the values measured about 10 times. The open symbols represent the result from neutron-irradiated specimens.

All electron-irradiated specimen showed the recovery of

thermal diffusivity from 400-500°C, and AlN specimens recovered linearly with the annealing temperature (Fig.1). The electron-irradiated β -SiC specimen (Fig.2) showed recovery from 400°C with quadric curve.

In the case of neutron-irradiated AlN, the onset temperature of recovery (800-900°C) is higher than and independent of the irradiation temperature. On the other hand, the electron-irradiated specimen recovered from 400-500°C, that is obviously lower than the onset temperature of recovery in neutron-irradiated specimens and higher than the irradiated temperature. The neutron-irradiated β -SiC showed almost same behavior as the electron-irradiated specimen at lower temperature. While the neutron-irradiated β -SiC recovered rapidly with quadric curve above 1000°C.

This difference may arise from the difference in the crystal structure discussed in a previous work, where the defect structure was explained by the pileup model (AlN) and nano-partition model (β -SiC).

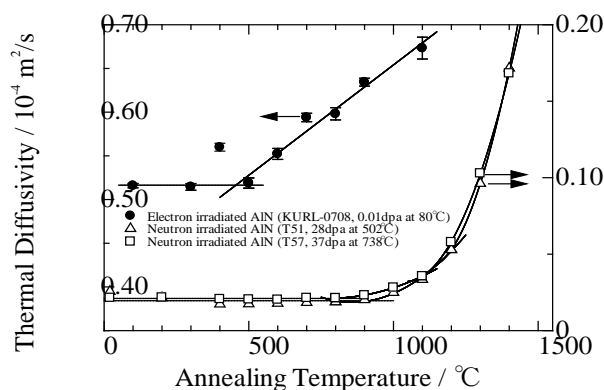


Fig.1 Recovery behavior of thermal diffusivity in electron-irradiated AlN ceramic with isochronal annealing.

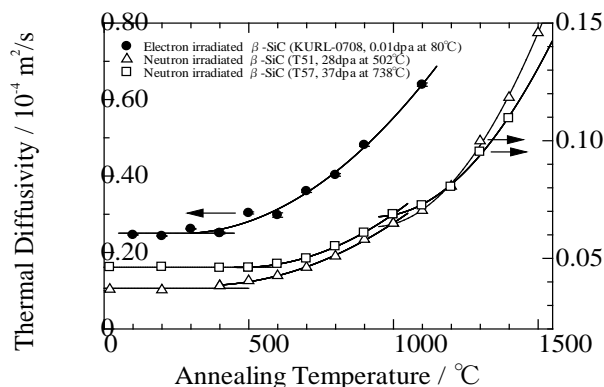


Fig.2 Recovery behavior of thermal diffusivity in electron-irradiated β -SiC ceramic with isochronal annealing.

PR1-6 Annealing Behavior of Vacancy-Type Defects in Mg-Zn-Y Alloy with LPSO Structure Introduced by Electron-irradiation at Liquid Nitrogen Temperature

Y. Nagai, K. Inoue, T. Toyama, Y. Matsukawa, Y. Shimizu, A. Kuramoto, H. Takamizawa, Y. Kakubo, T. Yoshiie¹, Q. Xu¹ and K. Sato¹

Institute for Materials Research, Tohoku University

¹Research Reactor Institute, Kyoto University

INTRODUCTION: Mg alloys containing transition-metal (TM) and rare-earth (RE) elements (Mg-TM-RE) have received a considerable amount of attention in recent years as a new-class of light-weight structural material that exhibits high strength and high ductility, simultaneously. A long-period stacking-ordered (LPSO) structure which is long period stacking variants of hcp-Mg by introducing the TM/RE enriched layers synchronized with stacking faults periodically have been believed to play a critical role in endowing such attractive mechanical properties and high ductility with the Mg-TM-RE alloys. In order to understand the detailed mechanisms for the formation, it is important to investigate the behavior of vacancy-type defects in the material with LPSO structure. Positron annihilation spectroscopy is well known to detect vacancy-type defects in materials. In this work we have investigated annealing behavior of defects introduced by electron-irradiation at liquid nitrogen temperature.

EXPERIMENTAL: The samples used in this study are Mg₈₅Zn₆Y₉ alloy with almost 100% LPSO structure. The samples were irradiated at 77K to a fluence of 4×10^{18} e/cm² using the KUR-LINAC. The samples were set to a sample chamber for positron annihilation (positron lifetime and coincidence Doppler broadening (CDB)) apparatus without temperature rise. The positron annihilation measurements were performed at 77K. The isochronal annealing was done for 5 minutes at 10K intervals.

RESULTS & DISCUSSION: Figure 1 shows annealing temperature dependence of mean positron lifetime. In as-irradiated state, the mean positron lifetime is 283 ps, which is much longer than the un-irradiated state (223 ps). Almost all the positrons are trapped at vacancy-type defects introduced by electron-irradiation in the as-irradiated state. Annealing behavior of the mean positron lifetime consists of several stages as shown in Fig. 1. The lifetime starts to decrease above 120K and decrease largely until 160K. It decreases gradually from 160K to 250K and is almost constant from 250K to 300K and decreases again above 300K. It is reported that the divacancy and monovacancy can migrate at 130K and 160K

in pure Mg, respectively [1]. Therefore, large decrease of the mean positron lifetime above 120K to 160K probably corresponds to the recovery of the divacancy in hcp-Mg layer of the LPSO structure and gradual decrease from 160K to 250K corresponds to the recovery of the monovacancy in hcp-Mg layer of LPSO structure and formation of the higher order vacancy complexes.

The correlation between low momentum component fraction (LMCF: $|p_L| < 4 \times 10^{-3} mc$) and high momentum component fraction (HMCF: $14 \times 10^{-3} mc < |p_L| < 23 \times 10^{-3} mc$) in CDB spectrum are shown in Fig. 2, where p_L denotes the momentum, m is the electron/positron rest mass, and c is the speed of light. In the as-irradiated state, LMCF-HMCF correlation point shift not toward lower-right direction from the point of Mg but toward the point of Y. Therefore, Y atoms probably exist next to the vacancy. The correlation points move slightly toward the point of Zn above 120K, indicating the formation of vacancy-Zn complexes during the migration, and then move toward the point of Mg.

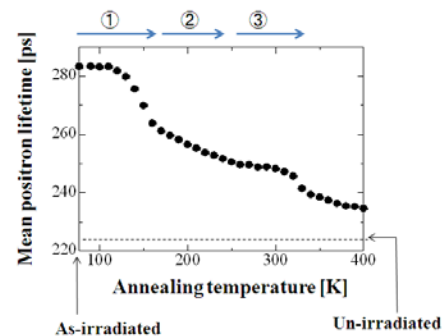


Fig. 1. Annealing temperature dependence of mean positron lifetime.

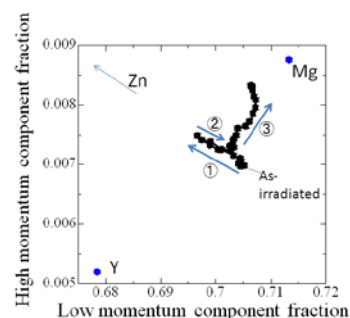


Fig. 2. Annealing behavior of LMCF-HMCF correlation in CDB spectrum.

REFERENCES:

[1] P. Hautojarvi *et al.*, Appl. Phys., A **27** (1982) 49-56.

PR1-7 Radiation Damage in Bulk Amorphous Alloys by Electron Irradiation

F. Hori, N. Onodera, K. Ishii, A. Iwase, Y. Yokoyama¹,
Q. Xu², K. Sato² and T. Yoshiie²

Dept. of Mater. Sci., Osaka Prefecture University

²Institute of Materials Research, Tohoku University

¹Research Reactor Institute, Kyoto University

INTRODUCTION: It is well known that the irradiation damage of the metal under high-energy particles irradiation makes various effects with the alloy compositions. The amorphous alloys, which have no long-range atomic periodicity, are expected to be useful for various applications due to their superior mechanical properties such as hardness, strength, corrosion resistance and micro-formability. We have been studying the radiation effects of various kinds of high energetic particles irradiation, such as an electron, proton and ions, irradiation on free volume and mechanical properties of ZrCuAl bulk glassy alloy. We have measured X-ray diffraction, DSC, positron annihilation and bulk density measurements for before and after an electron irradiated samples.

EXPERIMENTS: A samples of $Zr_{50}Cu_{40}Al_{10}$ bulk metallic glass with 8 mm in diameter and 60 mm in length was prepared by a tilt casting technique. For positron annihilation measurements, alloy sample was cut into the size of about 0.5 mm thickness. 8 MeV electron irradiations with total doses from 4.0×10^{17} to 2×10^{18} e/cm² was performed for these alloys at 300 K by LINAC at Research Reactor Institute, Kyoto University. Irradiated samples were examined by X-ray diffraction, positron annihilation lifetime and coincidence Doppler broadening measurements at room temperature. The positron annihilation lifetime spectra consist of more than 3.0×10^6 counts. The positron lifetime spectra were analyzed by the POSITRONFIT and CONTIN-PALS II program. The CONTIN program provides the annihilation probability density function $f(\lambda)$.

RESULTS: Figure 1 shows the change of the positron annihilation probability density distribution

function $f(\lambda)$ of before and after electron irradiated sample of $Zr_{50}Cu_{40}Al_{10}$ bulk metallic glasses. In this figure, peak position of positron lifetime distribution increases and the shape of its profile becomes slightly sharpen. In our previous work, mean positron lifetime increases from 167 to 176 psec by 8 MeV electron irradiation with the fluence of 2×10^{18} e/cm² [1,2], i.e., their difference is about 9 psec. This value is consistent with the shift of positron lifetime distribution peak by the irradiation. Also, no peak separation can be seen by the irradiation. These indicate that the electron irradiation does not retain a vacancy type defect randomly, but the damages have some interactions with intrinsic open volume. Consequently, mean size of free volume grows.

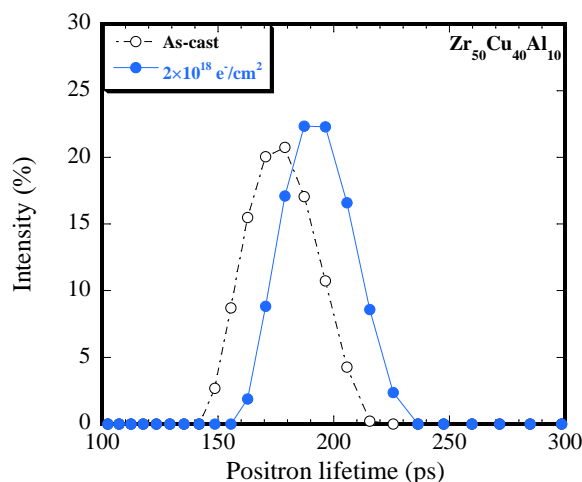


Fig. 1 Positron annihilation probability density function of as-prepared and after 8 MeV electron irradiated ZrCuAl bulk glassy alloy.

REFERENCES

- [1] F.Hori *et al.*, KURRI progress report 2011
- [2] Y.Fukumoto, A.Ishii, A.Iwase, Y.Yokoyama, F.Hori, J. Phys.: Conf. 225 (2010) 012010

PR1-8 Development of Replica Extraction Method for Vanadium Alloys and its Application for Neutron-Irradiated Ones

K. Fukumoto and Q. Xu¹

RINE, Univ. of Fukui

¹ Research Reactor Institute, Kyoto University

INTRODUCTION:

Vanadium-base alloys are attractive candidates of low activation structural materials for future fusion reactors. Since small Ti(OCN) precipitates were the dominant microstructural feature in neutron-irradiated V-4Cr-4Ti alloys at elevated temperatures, the precipitation processes of Ti(OCN) should be well understood. For this purpose, we have irradiated V-4Cr-4Ti alloy by neutrons to induce defect clusters due to displacement cascades and have studied the characterization of neutron-induced precipitates. Electron microscopy and microanalysis were employed to investigate the features and mechanisms of precipitation process in the V-4Cr-4Ti alloy under irradiation through knowledge the crystallography, chemical composition and size distribution of precipitates. A carbon replica technique has been developed to extract precipitates from vanadium alloys. Using this technique, precipitation phases can be extracted from neutron-irradiated or thermal-aged V-4Cr-4Ti alloys.

EXPERIMENTS: The majority of test specimens for this study were prepared from V-4Cr-4Ti alloys. Before irradiation, all specimens were annealed in vacuum at 1000°C for 2hrs. Neutron irradiation experiments were performed in the e JOYO reactor. Two irradiation conditions were selected to investigate the nature of irradiation-induced precipitates. The irradiation temperatures, irradiation doses and displacement damages for 1/3CVN specimen was intended to be 450°C, 2.3×10^{26} n/m² ($E > 0.1$ MeV) and 15dpa estimated for pure vanadium. Those conditions for S5J-3 specimen was intended to be 593°C, 1.7×10^{27} n/m² ($E > 0.1$ MeV) and 107dpa. The microstructural TEM observations were performed in KUR/Kyoto Univ.

The carbon replica technique yielded measurements of chemical compositions for irradiation-induced precipitates without matrix contribution. A mechanically polished surface of specimen was put into a chemical polishing solution for 30s. A carbon layer was sputtered on the specimen surface and then, an electro-etching procedure was performed in order to collect the replicas.

RESULTS: Fig.1 shows the TEM micrographs of neutron-irradiated V-4Cr-4Ti alloy at 593C with 105dpa. TEM micrographs reveal tangled dislocation structure and bimodal distribution of irradiation-induced precipitates such as Ti-(CON) precipitate with {100} habit plane. The crystal structure of precipitates could not be identified due to their fine size about few ten nm, but the previous work for neutron-irradiated V-Cr-Ti and V-Ti alloys have already reported that precipitate with {100} habit plane is identified to be the same structure as Ti-rich (CON) precipitate. Fig.2 shows the STEM image of tiny irradiation-induced precipitate on carbon replica film and Fig.6 shows the results of the chemical composition analysis of their precipitates using X-EDX. The chemical composition of titanium varied from 20% to 100% and vanadium and chromium consisted of the other composition. Thus the precipitate with {100} habit plane is no longer type of Ti-(CON) but MX type with M=(Ti, V, Cr) and X=(C, O, N). Even though the Ti-(CON) precipitate is in an equilibrium state, the MX type is in a metastable state during irradiation circumstance.

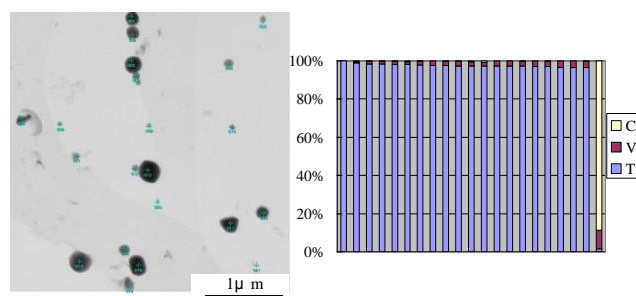


Fig.1. A set of (a) STEM bright image and spectrum of EDS analysis of the precipitate in as received V-4Cr-4Ti alloy

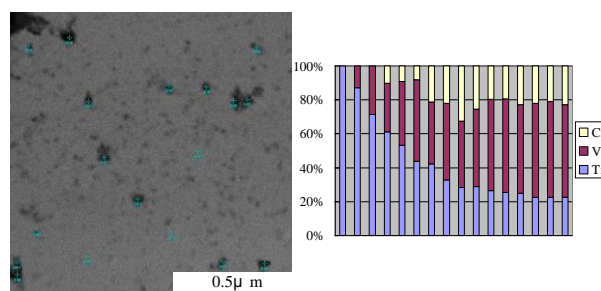


Fig.2. A set of (a) STEM bright image and spectrum of EDS analysis of the precipitate in neutron -irradiated V-4Cr-4Ti alloy at 593C with damage of 107dpa.

採択課題番号 24P1-8 中性子・イオン照射を用いたバナジウム合金の熱処理による プロジェクト
損傷回復過程

(福井大院工) 福元謙一 (京大・原子炉) 徐虫L

I. Mukouda, K. Yamakawa¹, T. Yoshiie² and Q. Xu²

Hiroshima International University

¹*Faculty of Engineering, Ehime University*

²*Research Reactor Institute, Kyoto University*

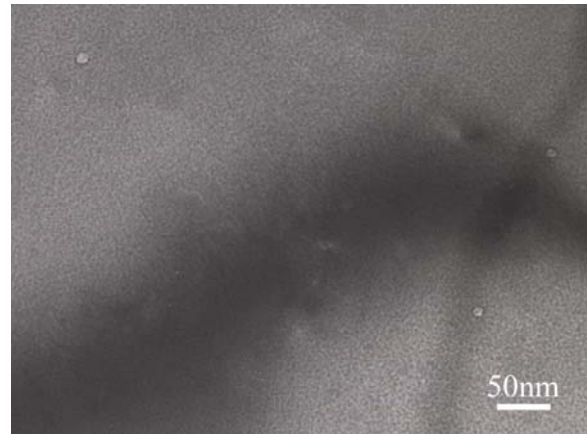
INTRODUCTION: Copper and nickel are used as typical FCC metals in radiation damage studies. Many studies have been carried out and reviewed by Singh and Zinkle [1]. They concluded that there is a lack of information on the microstructure of copper and nickel irradiated to below 10^{-2} dpa at 100 to 300°C [1]. Zinkle and Snead carried out fission neutron irradiation at 230°C to damage levels between 10^{-2} and 10^{-1} dpa [2]. They concluded that a high density of small SFT and dislocation loops was observed in copper and nickel, and small voids were observed in irradiated copper. Recently Shimomura and Mukouda carried out fission neutron irradiation of copper at 200 and 300°C at a similar range of dose, we reported dose dependence of voids and SFTs previously. The present work is carried out to examine the evolution of vacancy clusters and voids in neutron-irradiated copper of transient regime at elevated temperatures. To obtain precise results, the irradiation was carried out at the temperature controlled irradiation facility in the KUR.

EXPERIMENTAL PROCEDURES: The specimens used in this study were pure copper and nickel. Specimens were cold-rolled to 0.05 mm and punched out to disks of 3mm in diameter, and annealed in vacuum. Neutron irradiation was carried out in the temperature controlled capsule at KUR reactor in SSS at 1MW. The specimen temperature was kept at 300°C or 200°C during irradiation. After radiation cooling, specimens were electro-polished and using JEOL-2010 TEM at an accelerating voltage of 200kV. Void images were observed by bright field technique of off-Bragg diffraction condition (void contrast) and weak beam dark field (WBDF) image.

RESULTS AND DISCUSSIONS: Figure 1 shows TEM observation of neutron- irradiated copper at 300°C, 5.7×10^{17} n/cm², by bright field image. Large voids were seldom observed in this specimen. Fig. 2 shows TEM observation of same specimen by dark field image. Large SFT and small interstitial clusters were observed. The number density of voids and point defect clusters were smaller than irradiation at 5MW 300°C specimen [3]. Fast neutron flux was 1.7×10^{13} at 5MW, 3.4×10^{12} n/cm²s. Another irradiation conditions are progressing now.

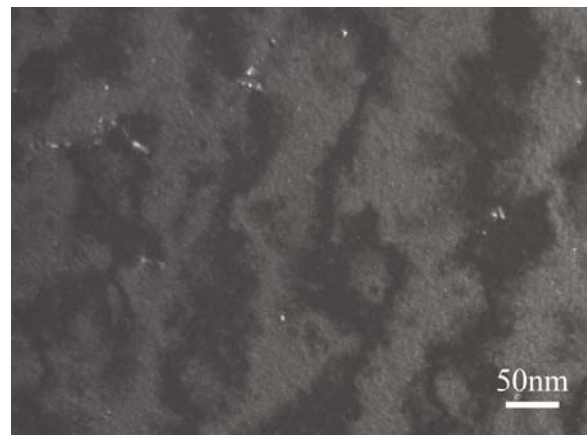
REFERENCES

- [1] B. N. Singh and S. J. Zinkle, *J. Nucl. Mater.*, **206**, 212 (1993).
- [2] S. J. Zinkle and L. L. Snead, *J. Nucl. Mater.*, **225**, 123 (1995).
- [3] I. Mukouda and Y. Shimomura, *Mat. Res. Soc. Symp. Proc.*, **650**, R3.11.1-R3.11.6 (2001)



KUR 1MW 300°C 47h

Fig. 1. TEM observation of neutron- irradiated copper at 300°C, 5.7×10^{17} n/cm², by bright field image.



KUR 1MW 300°C 47h

Fig. 2. TEM observation of neutron- irradiated copper at 300°C, 5.7×10^{17} n/cm², by dark field image, (g,5g) g=200.

PR1-10 Positron Annihilation Behavior of Fe-Cr Alloys after Neutron Irradiation in KUR

R. Kasada, K. Sato¹, Q. Xu¹ and T. Yoshiie¹

Institute of Advanced Energy, Kyoto University

¹Research Reactor Institute, Kyoto University

INTRODUCTION: Ferritic steels containing Cr are expected to be used for the first-wall component in the fusion reactors as well as the fuel pin cladding in the Generation IV nuclear fission systems [1]. However, high-Cr steels may suffer from thermal aging embrittlement, which is well-known 475 °C embrittlement. This is mainly due to phase separation of Fe and Cr as shown in the phase diagram (Fig.1). In the previous study [2], we applied a positron annihilation spectrometry to detect the phase separation in the Fe-Cr alloys under “the Strategic Promotion Program for Basic Nuclear Research by the Ministry of Education, Culture, Sports, Science and Technology of Japan”.

The present collaborative research has moved to investigate the neutron irradiation effect on the phase separation of Fe-Cr ferritic alloys. In the FY2012 we have obtained the first result of positron annihilation study on the Fe-Cr binary alloys before and after the neutron irradiation in KUR.

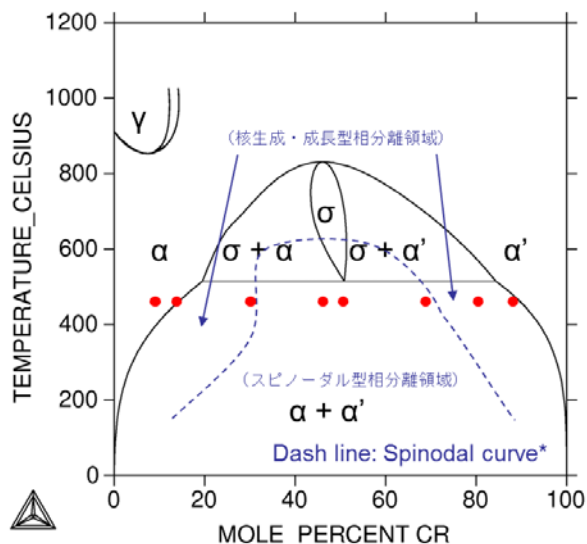


Fig. 1 Phase diagram of Fe-Cr binary system calculated using ThermoCalc software.

Experimental Procedure: Materials used in the present study is Fe-Cr binary alloys. Neutron irradiation on these materials was carried out at 300 °C up to 199 h in KUR. The displacement damage is 2.1×10^{-3} dpa (5.1×10^{18} n/cm²). Positron annihilation coincidence Doppler broadening (CDB) measurement were performed at the hot laboratory of KURRI.

Results and Discussions: The CDB ratio curves to pure Cr of Fe-30Cr alloy before and after the neutron irradiation is shown in Fig. 2. It should be noticed that the high-momentum region of the irradiated Fe-30Cr is close to that of unirradiated Fe. This means that the most of positron annihilates with the Fe electron in the irradiated Fe-30Cr. Considering with the positron annihilation behavior of the themally aged Fe-Cr alloys, the current irradiation condition may enhance the phase separation of Fe-30Cr alloy. Further experiments on the Fe-Cr alloys are now going.

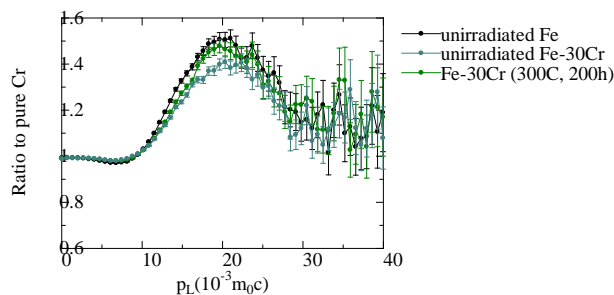


Fig. 2 Positron CDB ratio-curves obtained for the ODS steels and SUS430 before and after neutron irradiation at 300 °C up to 199 h.

REFERENCES:

- [1] A. Kimura, *et al.*, Journal of Nuclear Science and Technology, 44 (2007) 323-328.
- [2] R. Kasada and K. Sato, to be submitted.

H. Tsuchida, A. Itoh¹, K. Sato², T. Yoshiie² and Q. Xu²

Quantum Science and Engineering Center, Kyoto University

¹Department of Nuclear Engineering, Kyoto University

²Research Reactor Institute, Kyoto University

INTRODUCTION: Nanocrystalline (NC) materials are known to have high resistance to radiation damage effects, because the grain boundaries act as effective sinks that absorb radiation-induced defects. Up to the present, we have studied radiation damage in NC nickel under ion or neutron irradiation using positron annihilation spectroscopy. In the ion irradiation study, we investigated the dependence of the grain size on the formation of transient vacancy defects that occurred during irradiation in a real-time measurement of Doppler-broadening positron-annihilation spectroscopy [1]. It was found that the transient vacancies were unstable in NC materials and they could be annihilated at grain boundaries or via recombination with freely migrating interstitials during irradiation. In the neutron irradiation study, we investigated the grain size dependence on defect accumulation using positron annihilation lifetime spectroscopy. The results showed that for NC materials the defect accumulation is suppressed, whereas for coarse-grained materials, the defect accumulation or defect clustering is occurred with increasing the neutron fluence. These results suggest that grain boundaries play an important role in the mechanism of radiation resistance in NC materials.

In this work, we studied similarity of radiation resistance of NC Ni, in comparison between ion and neutron irradiation. It was found that defect accumulation near grain boundaries is suppressed both for ion and neutron irradiation.

EXPERIMENTS: An NC Ni, obtained from the Goodfellow Company, UK, was used as a specimen. The average grain size was 30 nm. The specimens were irradiated with neutron at the dpa 3.8×10^{-5} - 1.8×10^{-3} . Vacancy defects produced in the irradiated specimens were analyzed by positron annihilation lifetime spectroscopy. We also performed irradiation experiments with high-energy heavy ions. To measure vacancy defects produced during irradiation, the specimens were analyzed by in situ Doppler-broadening positron-annihilation spectroscopy.

RESULTS: We studied a change in microstructure NC Ni for neutron irradiation, and measured values of positron annihilation lifetime as a function of the dpa. We found that the value of the lifetime, corresponding to the positron annihilation occurring near grain boundaries, remain unchanged with increasing the dpa. This indicates

that the suppression of defect accumulation at grain boundaries occurs under neutron irradiation.

Next, we investigated the transient vacancies formed during irradiation via in situ observations of the positron annihilation Doppler broadening spectra. The annihilation line-shape parameter S was measured during and after irradiation. Fig. 1 shows experimental results for the variation of the line-shape parameter S measured alternately under irradiation (closed symbols) and non-irradiation (open symbols) conditions, for (a) the NC Ni irradiated with 0.5 MeV C ions, (b) the NC Ni irradiated with 2.5 MeV C ions, and (c) the coarse-grained Ni (annealed polycrystalline Ni) irradiated with 2.5 MeV C ions. The variation of S for the NC specimen was different from that observed for the coarse-grained specimen. For the coarse-grained specimens, the S measured during irradiation was larger than that observed before/after irradiation, while for the NC specimens, the S value remained unchanged. The results for the coarse-grained specimens indicated that the concentration of vacancies during irradiation was high compared with that after irradiation. This is due to that transient vacancy defects were produced during irradiation. In contrast, the results for the NC specimens suggested that such transient vacancies disappear, and the defect concentrations remain unchanged during irradiation. The results observed in the ion irradiation experiments shows the same trend to that in the neutron irradiation experiments. This similarity may be related to the defect annihilation occurring near grain boundaries.

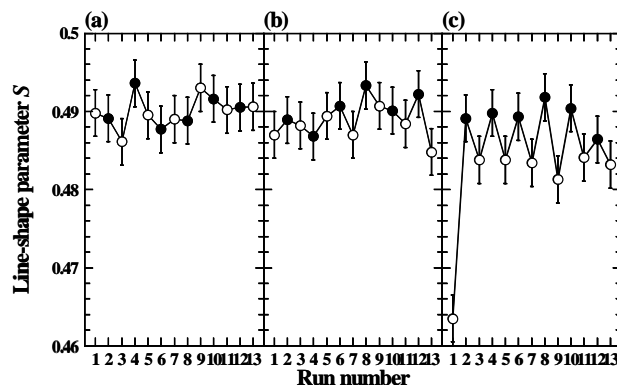


Fig.1 Variation of the line-shape parameter S measured alternately under irradiation and non-irradiation

REFERENCES:

[1] Tsuchida *et al.*, "Radiation damage in nanocrystalline Ni under irradiation studied using positron annihilation spectroscopy", J. Nucl. Mater., (2013) (accepted)

K. Sato, R. Tamiya¹, Q. Xu and T. Yoshiie

Research Reactor Institute, Kyoto University

¹Graduate School of Engineering, Kyoto University

INTRODUCTION: In a fusion reactor, plasma-facing materials (PFMs) must withstand the damage produced by hydrogen and helium at up to 10 keV of energy and heat loads from the plasma, in addition, the neutrons with high energy, high flux and high fluence similar to the structural components. Hydrogen isotopes retain in vacancy-type defects in PFMs, and this is a critical problem for fusion reactors. To know the interaction between vacancy-type defects and hydrogen isotopes is very important. In this study, the size and density of vacancy-type defects in tungsten was obtained by positron annihilation lifetime (PAL) measurements. Next, thermal desorption spectra of deuterium was obtained after deuterium charging. From these results, trapping site and dissociation energy of deuterium were identified.

EXPERIMENTS: The samples were 99.95% pure tungsten (A.L.M.T. Corp.). The 0.2-mm-thick sheet was punched to 5mm in diameter. These samples were annealed at 1773 K for 1 h in a vacuum of less than 10^{-4} Pa. Electron and deuterium ion irradiations were carried out to introduce defects. Electron irradiation was performed at Electron Linear Accelerator of Research Reactor Institute, Kyoto University. 8 MeV electrons were irradiated up to $9.4 \times 10^{17} / \text{cm}^2$ (1.3×10^{-4} dpa). A displacement threshold energy used for irradiation dose calculation was 42 eV [1]. Deuterium ion irradiation was performed at Low-energy ion irradiation system of Research Reactor Institute, Kyoto University. 5 keV D_2^+ ions were irradiated up to $1.0 \times 10^{18} / \text{cm}^2$ (20 dpa at defect peak) at room temperature (R.T.). Iron ion irradiation was performed at 2.0-MV tandem accelerator of Quantum Science and Engineering Center, Kyoto University. 6 MeV Fe^{3+} ions were irradiated up to $2.3 \times 10^{19} / \text{cm}^2$ (8.4 dpa at defect peak) at 573 K. After that, 1 keV D_2^+ ions, which do not form irradiation defects, were implanted by low-energy ion irradiation system. Thermal desorption spectroscopy was carried out from R.T. to 1523 K in order to detect elimination behavior of deuterium from tungsten.

RESULTS: TDS spectra of electron-, 5 keV- D_2^+ ion- and 6 MeV- Fe^{3+} ion-irradiated samples are shown in Fig. 1. From PAL measurement, single vacancies are detected in electron-irradiated sample. Therefore, peak around 550 K denotes elimination of deuterium from single vacancies. Peak separation analysis was performed to spectra of 5 keV D_2^+ ion- and 6 MeV Fe^{3+} ion irradiation by data analysis software Origin, and the results were shown in Figs. 2 and 3. Spectra of 5 keV D_2^+ ion irradiation at R.T. were resolved into three gauss functions. The peak of them was around 450 K, 560 K and 640 K. Spectra of 6 MeV Fe^{3+} ion irradiation at 573 K were also resolved into

three gauss functions. The Peak of them was around 460 K, 630 K and 840 K. 450 K peak denotes the elimination of deuterium from surface. It is expected that 560 K peak denotes the elimination of deuterium from single vacancies from result of electron-irradiated sample. 640 K peak denotes the elimination of deuterium from dislocations. 840 K peak denotes the elimination of deuterium from voids. It is not clear that voids are formed during iron ion irradiation or increase in temperature of TDS measurement.

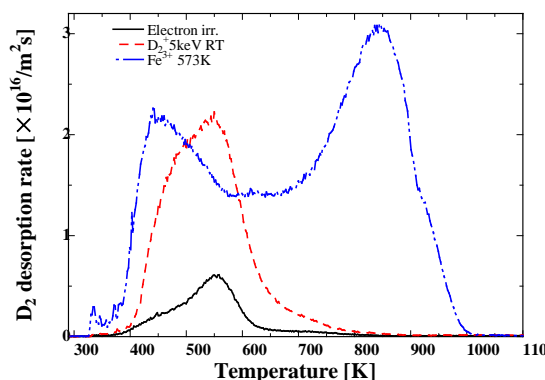


Fig. 1. TDS spectra of electron-, 5keV D_2^+ ion-, 6MeV Fe^{3+} ion-irradiated samples

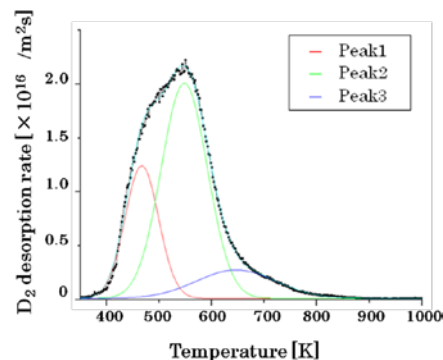


Fig. 2. Peak separation of TDS spectrum of sample irradiated with 5 keV D_2^+ ions at R.T.

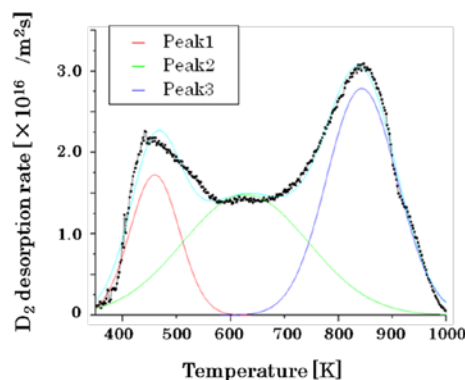


Fig. 3. Peak separation of TDS spectrum of sample irradiated with 6MeV Fe^{3+} ions at 573 K.

REFERENCES:

[1] F. Maury, M. Biget, P. Vajda, A. Lucasson and P. Lucasson, Radiat. Eff. 38 (1978) 53.

K. Tokunaga, K. Araki, T. Ukita¹,
Q. Xu² and T. Yoshiie²

Institute for Applied Mechanics, Kyushu University

¹*Interdisciplinary Graduate School of Engineering
Sciences, Kyushu University*

²*Research Reactor Institute, Kyoto University*

INTRODUCTION: Tungsten (W) is the primary candidate for use as plasma facing materials/components (PFM/PFC). PFM/PFC will be subjected to heavy thermal loads in the steady state or transient mode combined with high energy neutron irradiation that will cause serious material degradation. It is necessary to clarify mechanical strength to evaluate thermal behaviour of tungsten materials by high heat loading. In the present works, the tensile testing of W material has been performed up to at 1600 °C to obtain stress-strain curves. In addition, thermo elasto-plastic stress analyses of W specimen have been carried out to evaluate modification of the W specimen exposed to high heat loading. Furthermore, the calculated results have been compared to surface modification of W specimen under cyclic thermal loading experiments using an electron beam to evaluate thermo-mechanical performance of W.

EXPERIMENTS: W material used in the present work was ITER grade W. Tensile testing was performed on dog-bone shaped tensile test specimens with an overall length of 16 mm, a gauge length of 5 mm and an effective cross section of 0.6 mm². The orientation of the specimens used were parallel (L-R type) and perpendicular (T-R type) directions to rolling direction along rolling surface, respectively. The tests were conducted at RT, 200, 400, 650, 800, 1000, 1300, 1600 °C. The tests were performed at a strain rate of $2 \times 10^{-4} \text{ s}^{-1}$. In addition, ITER grade W was machined to the dimensions of 10 mm x 10 mm x 1mm, followed by mechanical and electro polishing. The polished specimens were subjected to high heat load experiments by an electron beam irradiation test simulator. The experiments were conducted at the irradiation conditions; repeated irradiations of 2 s-irradiation and 7.5 s-rest with one cycle of 9.5 s for totally 200 times. The surface temperature of the specimens changes from below 450°C to 1300°C by 2 s-irradiation. Before and after the irradiation, the specimen surfaces were examined by SEM. The thermo elasto-plastic stress analyses using a transient finite element analyses (FEA) have been performed to evaluate the thermal behaviour and surface modification of the W specimens during the high heat loading experiments. Stress-strain curves of ITER grade

W have been obtained by the tensile testing used in the FEA.

RESULTS: Figure 1 shows stress-strain curves of ITER grade W (L-R type) with various temperatures. Brittle fracture occurs both L-R and T-R type specimens at RT. On the other hand, ductile fracture occurs on L-R type specimen but not T-R type specimen at 200 °C. This result means that DBTT of the specimen is around at 200 °C in the case of the strain rate. Yield strength decreases and total elongation increases with increasing test temperature. There is difference of about 100 MPa between L-R and T-R type specimens on tensile strength at RT and 200 °C, however, there is no difference between them above 400 °C. The reason for this is considered that migration of dislocation do not occurs at low temperature, and shape of grain boundary for direction of stress influences tensile strength. On the other hand, there is difference between L-R and T-R type specimens on total elongation, even if high temperature which ductile fracture occurs, and total elongation of L-R type specimen is higher than that of T-R type specimen. The repeated heating by electron beam irradiations of 20 times caused surface roughening in the intragranular. The subsequent repeated irradiations of totally 200 times caused significant surface roughening, cracking in the intragranular and grain boundaries and surface exfoliation. The FEA indicated that compressive stress is generated in the electron beam irradiated area during the electron beam irradiation. On the other hand, tensile stress is generated during cooling after the irradiation of the electron beam is ended. In addition, plastic deformation occurs and residual stress remains in the W specimen. Those results suggest that the surface roughening is considered to be caused due to plastic deformation by the thermal stresses. Irradiation effect for stress loading property is planning to be investigated in the next stage.

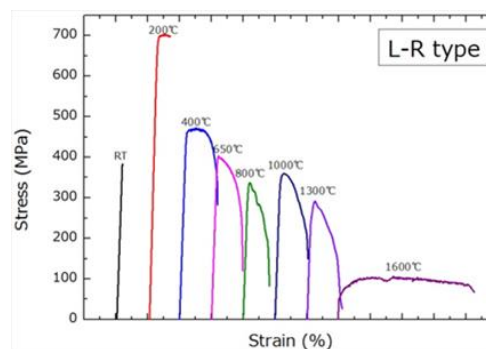


Fig. 1 Stress-strain curves of ITER grade W (L-R type) with various temperatures.

N. Nitta, K. Yokoyama and M. Taniwaki

Department of Environmental Systems Engineering, Kochi University of Technology

INTRODUCTION

The authors proposed a novel nanofabrication technique and have performed to fabricate nanocell lattices by focused ion beam (FIB) at room temperature. In their past studies, mainly the possible range of the cell interval and ion dose yielding ordered nanocell lattices has been obtained only at room temperature. However, the mobility of the point defects, which dominates the nanocell formation, depends strongly on the temperature, then, the range of the parameters for successful nanocell formation must differ so much by substrate temperature. Then, in this work, the authors investigated the effect of the substrate temperature by fabricating nanocell lattices on GaSb (100) surface at room temperature and at lower temperature (130 K) and comparing them.

EXPERIMENT

Nanocell lattices were fabricated using FIB Quanta 3D 200i by the nanofabrication technique that the authors had proposed. In order to know the possible range of the cell interval for the ordered nanocell lattice, an initial pattern consisting of nine matrices with a different void interval was created by the same ion dose per one dot in box repairing mode of the FIB with 30 keV Ga⁺ and it was developed by a constant ion dose per unit area in the image scanning mode of the same FIB. Such processes were performed in variations of initial ion dose and developing ion dose at room temperature and 130 K. The ion doses per one dot in the initial procedure were 1.13×10^4 - 2.25×10^6 ions/dot and the ion doses per unit area in the second procedure were 1.6×10^{13} - 2.9×10^{14} ions/cm². The change of the pattern during irradiation was observed in situ by FIB secondary electron image.

RESULTS

The lattice image of the pattern at 130K is observed obscurely, which may be due to the gas adsorption on the surface. The dot contrast is bright on the sample fabricated at 130K in contrast to the dark image on the sample at room temperature. The bright contrast means the elevation of the surface. This is due to the low migration of vacancies at cryogenic temperature, which retards the growth of void comparing at room temperature and then the top surfaces of the voids were not yet completely removed. The ordered image at 130 K was observed in the dot interval of 80 nm which was not made at room temperature. The development of the pattern by scanning at 130 K was re-

tarded comparing at room temperature, which is again attributed to the difference in the migration of point defects, especially vacancies. The cell diameter in one scanned pattern was larger in larger dot interval, and 55 – 108 nm at 130 K and 90 – 125 nm at room temperature. It increased monotonously with increasing scan times in every lattice at both temperatures, though it saturated to a critical value a little less than its dot interval. However, some difference is observed between two substrate temperatures; the curve of cell diameter against scan times is a convex below at 130 K, and linear or a convex on the top at room temperature. The increasing rate of the diameter to scan times at early scanning stage is 7.8 nm/one scan at 140 K and 13.7 nm/one scan at room temperature. We consider that this difference may be caused by the difference of the nanocell development mechanisms (probably it contains two elementary mechanism at least) between at room temperature and at cryogenic temperature. This detailed understanding is our future issue.

CONCLUSION

The nanocell fabrication experiment on GaSb (100) using 30 keV Ga⁺ at room temperature is summarized as follows. The appropriate ion dose for fabrication of the initial void is $1.13 - 2.25 \times 10^5$ ions/dot, and nanocell lattice with 80 – 300 nm dot interval is achieved. The nanocell fabrication on GaSb surface at low temperature has several advantages over that at room temperature. One is to suppress the secondary void formation. In the case of 130 K, secondary voids formed first by 8 scans, though they formed by 5 scans at room temperature and their size was smaller at 130 K. Another advantage at low temperature is to create the ordered nanocell lattice with smaller dot interval. Nanocell formation mechanism at cryogenic temperature is somewhat different from that at room temperature. Fabrication at low temperature has some advantages in application, that is, nanocell lattices are easily obtained in wider range of dot interval, without secondary void formation.

*This report is summarized from “Nanocell fabrication on GaSb at room temperature and cryogenic temperature (N. Nitta, K. Yokoyama, and M. Taniwaki, AIP conf. Proc. 1496)

Y. Hatano, J. Shi, T. Nozaki, K. Masuda, T. Tokunaga¹,
H. Watanabe¹, N. Yoshida¹, K. Sato² and Q. Xu²

Hydrogen Isotope Research Center, University of To-
yama

¹Research Institute for Applied Mechanics, Kyushu
University

²Research Reactor Institute, Kyoto University

INTRODUCTION: Tungsten (W) is currently recognized as a primary candidate of plasma-facing material (PFM) for future fusion reactors. Vacuum plasma spraying is a technique to prepare W layers on structural materials such as reduced-activation ferritic/martensitic steels. Tritium (T) is the radioisotope of hydrogen and used as fuel in fusion reactors together with deuterium (D). The fusion reaction of D and T forms 3.5 MeV He and 14 MeV neutrons. PFMs are subjected to irradiation of those high energy neutrons. Therefore, understanding of T retention in PFMs and effects of neutron irradiation is important issue for assessing safety margins of fusion reactors. Indeed, significant increase in D retention with neutron irradiation has been observed for bulk W fabricated by powder metallurgy in Japan-US Joint Research Project TITAN [1–2]. From these viewpoints, effects of displacement damages on D retention in VPS-W were examined in this study with irradiation of 8 MeV electrons. High energy electrons induce defects throughout the thickness of materials like neutrons, while ions form defects only in a shallow region beneath the surface.

EXPERIMENTS: The specimens used were VPS-W layers (0.6 mm thickness) prepared on carbon/carbon-fiber composite (CFC, CX-2002U) by Plansee Aktiengesellschaft. After removing CFC substrates by mechanical polishing, the VPS-W layers were exposed to D₂ gas in a high-vacuum device at 100 kPa and 673 K for 10 hours under the following conditions:

- (1) As-received,
- (2) After heating in vacuum at 1273 K for 1.5 hours,
- (3) After irradiation with 8 MeV electrons up to 10⁻³ displacement per atom (dpa) following the above-mentioned heat treatment in vacuum.

Exposure to D₂ gas under several different conditions showed that the specimens were saturated with D under the above-mentioned conditions. The D retention was measured by thermal desorption spectroscopy (TDS) at the temperature ramp rate of 0.5 K s⁻¹. Desorption spectra were simulated with the program TMAP4 [3].

RESULTS: The retention of D in VPS-W layer under as-received conditions was 1 × 10⁻⁵ in atomic ratio, [D]/[W]. It decreased to [D]/[W] = 1 × 10⁻⁶ by the heat treatment in vacuum at 1273 K. During the heat treatment,

the desorption of CO was observed. Hence, the reduction in D retention by the heat treatment was ascribed to the removal of impurities such as carbon and oxygen acting as trapping sites against hydrogen isotopes. The electron irradiation resulted in increase in D retention to [D]/[W] = 3 × 10⁻⁵. In other words, D retention increased by an order of magnitude with irradiation as low as 10⁻³ dpa. Such significant increase in D retention was ascribed to trapping by radiation defects. Damage levels in ITER and demonstration reactors are expected to be far higher. Hence, T retention could be dominated by trapping effects by radiation defects.

Fig. 1 shows TDS spectrum of D from the electron-irradiated specimen together with the result of simulation with the TMAP4 program. The desorption peak from the electron-irradiated specimen was broad and it indicates long-range diffusion under trapping effects. The maximum desorption rate was observed at 830 K. The simulation roughly reproduced this peak temperature by setting the activation energy of detrapping to 1.5 eV. This value corresponds to detrapping from vacancies [4]. It is plausible that vacancies induced by the electron irradiation played dominant roles in trapping effects under the present conditions.

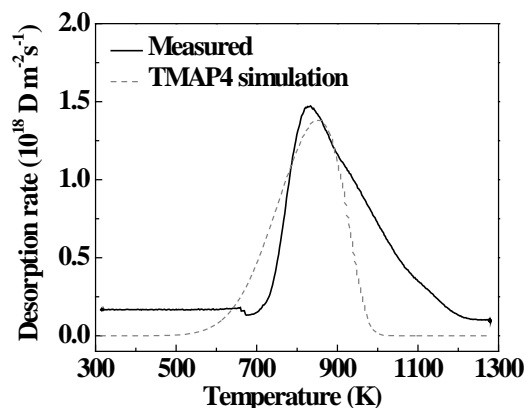


Fig. 1 TDS spectrum of D from electron-irradiated VPS-W and the result of simulation with the TMAP4 program, in which the activation energy for detrapping was set to 1.5 eV.

REFERENCES:

- [1] Y. Hatano *et al.*, Mater. Trans., **54** (2013) 437.
- [2] Y. Hatano *et al.*, J. Nucl. Mater., in press (doi: 10.1016/j.jnucmat.2013.01.018.)
- [3] G. R. Longhurst *et al.*, TMAP4 User's Manual, EGG-FSP-10315, doi: 10.2172/7205576.
- [4] H. Eleveld and A. van Veen, J. Nucl. Mater., 212-215 (1994) 1421.